

# Convective and Radiative Heating for Vehicle Return from the Moon and Mars

Robert B. Greendyke  
ViGYAN, Inc.  
Hampton, VA 23666

and

Peter A. Gnoffo  
NASA Langley Research Center  
Hampton, VA 23681-0001

## ABSTRACT

The aerothermal environment is examined for two vehicle forebodies near the peak heating points of Lunar and Martian return-to-Earth trajectories at several nominal entry velocities. The first vehicle forebody is that of a  $70^\circ$  aerobrake with 13.7 m diameter for entry into Earth orbit; the second, a capsule of Apollo configuration with 3.95 m diameter for direct entry into the Earth's atmosphere. The configurations and trajectories are considered likely candidates for such missions. Two-temperature, thermochemical nonequilibrium models are used in the flowfield analyses. In addition to Park's empirical model for dissociation under conditions of thermal nonequilibrium, the Gordiets kinetic model for the homonuclear dissociation of  $N_2$  and  $O_2$  is also considered. Temperature and emission profiles indicate nonequilibrium effects in a 2 to 5 cm post shock region. Substantial portions of the shock layer flow appear to be in equilibrium. The shock layer over an aerobrake for return from the moon exhibits the largest extent of nonequilibrium effects of all considered missions. Differences between the Gordiets and Parks kinetic model were generally very small for the lunar return aerobrake case, the greatest difference of 6.1% occurring in the radiative heating levels.

## INTRODUCTION

In recent years much effort has been devoted to improve the understanding and modelling of thermochemical nonequilibrium processes in high temperature shock layers. These shock layers form in front of vehicles travelling at hypersonic speeds through Earth and other planetary atmospheres. As the vehicle decelerates due to atmospheric drag, kinetic energy of the vehicle is transferred to

the gas, initially through an increase in translational temperature. The translational energy of the gas particles is redistributed among other modes of energy accommodation (i.e. vibration, electronic excitation, dissociation, ionization) through collisions. If the gas is sufficiently dense, collisions occur so frequently that energy accommodation quickly achieves an equilibrium distribution among modes that can be characterized as a function of two thermodynamic variables (i.e. temperature and pressure). A relatively simple equation of state is used to relate pressure, temperature and density in these equilibrium conditions. As gas density decreases, time between collisions increases and the nearly instantaneous accommodation of energy can no longer be assumed. In this case, the state of the gas is a function not only of local conditions, but is a net result of processes occurring as it traversed the flowfield. Simple state equations must now be replaced by partial differential equations.

Nonequilibrium processes influence the design of a hypersonic entry vehicle in three ways. Aerodynamics are effected because surface pressure distributions in compressing or expanding flows are a function of the heat capacity of the gas. Furthermore, laminar boundary layer thickness, which influences control surface effectiveness, is a function of gas chemistry. Examples of these aerodynamic effects are discussed in References [1] and [2]. Convective heating levels are effected by the degree of dissociation in the near wall region and the catalytic efficiency of the surface. Experimental and computational evidence of this effect are presented in References [3, 4, 5]. Finally, if gas temperature is sufficiently high, radiant energy transfer becomes an important mechanism for both cooling the shock layer (photons escaping the shock layer) and heating the vehicle surface. Proper modelling of nonequilibrium radiation is particularly important in the design of a lunar aerobrake because the total heat load is near the limit of a reusable thermal protection system [6].

The chemical kinetic models for air under conditions of thermal equilibrium and at temperatures and pressures that characterize the conditions in a shock layer surrounding a vehicle returning to earth from low earth orbit have been thoroughly investigated in ground based facilities. The validation of chemical kinetics under conditions of thermal nonequilibrium and at condition corresponding to shock velocities greater than 12 km/sec have been less extensive because of difficulties in performing the experiment. Reviews of such experimental data are presented in References [7] and [8]. Recent experimental contributions to this goal are presented in References [9, 11]. Validation of physical models also employs flight data [12, 13]. Of the available experimental data, the most difficult to match is associated with radiation. Though much progress has been made in recent years, there is no single set of models which is known to match all the available data.

Much work remains to be done toward validation of kinetic models under the conditions noted above. In order to provide more focus on such work, benchmarks have been assembled that are representative of vehicle size and freestream conditions at maximum heating for entry into the Earth's atmosphere on return from the Moon and Mars. These benchmarks serve to define the convective and radiative heating levels using a baseline thermochemical kinetic model. They focus on stagnation point heating only, and do not encompass issues relating to integrated heat load or base heating. They are intended to complement conditions frequently used in the validation process for which experimental data are available but which are not necessarily representative of most likely flight conditions. As kinetic models evolve, they can be tested at these benchmark conditions to assess their impact on vehicle aerothermodynamics. A comparison of two models for homonuclear dissociation rates under conditions of vibrational nonequilibrium are presented for one of the benchmark cases.

## VERSION

The Langley Aerothermodynamic Upwind Relaxation Algorithm (LAURA 4.0.4) is applied. It is a precursor to LAURA 4.1 (References [14, 15, 16]). Except for some numerical parameter defaults and application of a cell aspect ratio scaled limiter, which are defined below, the two versions are identical for the parametric variables of this study.

## CONFIGURATION

The aerobrake configuration used in this study is a spherically blunted,  $70^\circ$  semiapex cone with a nose radius,  $R_N$ , of 3.048 m. The base plane radius,  $R_B$  is 6.858 m., and the edge radius of the shoulder,  $R_S$ , is 0.3048 m. The capsule forebody geometry is identical to the Apollo Command Module. The capsule has an  $R_N$  of 4.595m. with an  $R_B$  of 1.975 m., and an  $R_S$  of 0.186 m. The configuration profiles are shown in Figure 1.

## GRID

The axisymmetric solution option within the LAURA code was chosen for both forebodies in this study. A preliminary grid refinement study was done using baseline LAURA parameters to determine a grid configuration for both vehicles that essentially yields grid independent solutions with fewest grid points. The best grid configuration tested was found to be 80 cells in the direction normal to the surface by 40 cells in the streamwise direction. The cell Reynolds number was set to 1.0 at the wall. An intermediate setting for shock grid adaption of “ep0=25/8” was used. While the radiative heat transfer calculations were more accurate with increased grid adaption, it was found for the conditions in this study that the results were only slightly affected when the maximum shock grid adaption parameter was used (“ep0=25/4”); however, use of this value had a small adverse effect on the calculation of the convective heat at the wall by pulling away grid points from the inner boundary layer. Additional guidance for grid adaption in such cases are detailed in Reference [6].

## CASE DENOTATION

Two basic mission profiles were used for this study. The first was a lunar return mission, and the second, a martian return mission. For each mission two vehicle options were studied. The aerobrake option called for a high altitude aerobraking pass followed by an entry into low Earth orbit. The capsule option called for the jettisoning of the “mother” vehicle in space and a return

directly to the Earth in a capsule carrying only the crew and important payloads. Three nominal entry velocity trajectories were available for each Martian return vehicle; there was only one nominal entry velocity choice for Lunar return - 11 km/s. In addition, two trajectory paths were available for each case, a fast “steep” trajectory, and a slower “shallow” trajectory. In order to simplify the study, the peak heating points at each nominal entry velocity were used. Further, to examine conditions of maximum and minimum nonequilibrium, the steep trajectories were examined for the aerobrake cases, while the shallow trajectories were used for the capsule configurations. Therefore, eight cases were examined in this study and each was assigned a six lettered case identifier. The first character (“l” or “m”) denotes the lunar or martian return profile. The second character (“a” or “c”) denotes either the aerobrake or capsule vehicle. The third and fourth denote the nominal entry velocity rounded to the nearest kilometer per second. Finally, the last two characters (“st” or “sh”) denote a steep or shallow trajectory.

## FREESTREAM CONDITIONS

Several sets of freestream conditions for the peak heating points were tested as shown in Table 1 with their case identifier.

Table 1 - Freestream Conditions

case	$V_\infty$ m/s	$\rho_\infty$ , kg/m <sup>3</sup>	$T_\infty$ , K	$h$ , km
la11st	9772.7	$7.1208 \cdot 10^{-5}$	217.	71.1
lc11sh	10050.	$9.3101 \cdot 10^{-5}$	222.	69.2
ma11st	10472.	$1.2270 \cdot 10^{-4}$	227.	67.1
ma12st	11504.	$1.0178 \cdot 10^{-4}$	224.	68.5
ma14st	12999.	$8.1436 \cdot 10^{-5}$	219.	70.1
mc11sh	10606.	$7.3453 \cdot 10^{-5}$	217.	70.9
mc12sh	11528.	$8.3948 \cdot 10^{-5}$	220.	69.9
mc14sh	12911.	$9.6000 \cdot 10^{-5}$	223.	68.9

## GAS MODEL

The test gas is air in thermal and chemical nonequilibrium. The laminar, thin-layer Navier-Stokes option was selected for all cases. An 11 species air model was tested including the species;  $N$ ,  $O$ ,  $N_2$ ,  $O_2$ ,  $NO$ ,  $NO^+$ ,  $N^+$ ,  $O^+$ ,  $N_2^+$ ,  $O_2^+$ , and  $e^-$ . The baseline gas kinetic model (“kmodel” set to 3 in line 23 of file “air.f”) is substantially derived from the work of Park as detailed in Table 1 of Reference [17]. However, the average vibrational energy released or absorbed by dissociation and recombination was changed in this study to be equal to be  $0.3 * D$  (see Eq. 3.42c of Reference [7]) from the baseline model in the LAURA code (version 4.0.4).

## GORDIETS GAS MODEL

The baseline Park model (Reference [17]) for nonequilibrium dissociation rates was compared with the Gordiets model (Reference [18]) for the la11st case. The Gordiets model is derived from a more complete physical model of the collision process. In the Gordiets model for homonuclear dissociation, where vibrational nonequilibrium exists the dissociation rate can be expressed as a functional dependence between the nonequilibrium dissociation rate ( $k$ ), the equilibrium rate of dissociation ( $k^\circ$ ), and  $T$  and  $T_V$ :

$$k(T, T_V) = k^\circ(T) \times \frac{1 - \exp(\frac{-\theta}{T_V})}{1 - \exp(\frac{-\theta}{T})} \times \exp[-(D - \beta T)(\frac{1}{T_V} - \frac{1}{T})] \quad (1)$$

where  $T$  and  $T_V$  are the translational and vibrational temperatures,  $\theta$  is the characteristic vibrational temperature,  $D$  is the dissociation energy, in degrees, and  $\beta$  is a dimensionless parameter. Empirical studies discussed in References [18, 8] indicated that  $\beta$  should be equal to 1.5 of the dissociation of  $O_2$ , and 3.0 for  $N_2$  dissociation. The Jacobian in subroutine “source.F” had to be modified to reflect the change in the gas model in the solution procedure.

In contrast, the baseline Park model uses:

$$k(T, T_V) = k^\circ(T_d) \quad (2)$$

where  $T_d = T^{0.7}T_V^{0.3}$ .

## BOUNDARY CONDITIONS

Standard, no-slip boundary conditions were set automatically by the “PRELUDE” program in the LAURA 4.0.4 package. In addition, a wall temperature option wherein the temperature at the wall is set equal to the equivalent radiative equilibrium temperature was used in combination with Stewart’s finite rate catalysis.

## NUMERICAL PARAMETERS

Solutions were started with eigenvalue limiter  $\epsilon_0 = 0.40$ , aspect ratio scaling across the boundary layer, and upwind limiter function as defined in Ref. [19]. After several grid adjustments, and when convergence was well underway, the eigenvalue limiter was reset to  $\epsilon_0 = 0.30$  and the grid was allowed to realign with the new limiter value. No changes to these parameters were made for any of the test cases, including the case run with the Gordiets model.

# RADIATIVE HEAT TRANSFER CALCULATIONS

The NEQAIR II code (Reference [20]) was used for all radiative heat transfer calculations. The output data from the LAURA code was reformatted to the correct input format for the NEQAIR II code. A stagnation streamline calculation was done using the tangent slab approximation method in the NEQAIR II code. The spectral matrix was set at 50,000 points for the region from 800 to 15,000 Angstroms for all calculations.

## RESULTS

In Figure 2, the convective heat profiles along the forebody of the aerobrake vehicle on a Martian return mission are plotted. The stagnation point convective heating for the 11, 12, and 14 kilometers per second nominal entry velocities are, respectively; 87.6, 109.5, and 135.8  $W/cm^2$ . All profiles exhibit a local minimum in their convective heating at the point on the forebody where the spherical nose section merges with the 70° conical body. This behavior is typical of flowfields where the sonic line sits on the spherical nose region. In undissociated air with a ratio of specific heats equal to 1.4, the sonic line sits over the aft corner of a 70 degree blunted cone. However, because of the small value of specific heat ratio for the high temperature, dissociated shock layer, the sonic line will jump forward to the spherical nose, causing a slight overexpansion at the sphere-cone junction and the observed trend in heating. Convective heat transfers for the Martian return capsule are plotted in Figure 3, with stagnation convective heating for the 11, 12, and 14 kilometer per second cases being 62.9, 86.4, and 127.8  $W/cm^2$ , respectively. Similar profiles are observed for the Lunar return aerobrake (Figure 4) and the Lunar return capsule (Figure 5) missions. Their stagnation point convective heat transfers are 52.7  $W/cm^2$  for the aerobrake, and 64.3  $W/cm^2$  for the capsule.

Stagnation streamline temperature profiles for the Martian return missions are plotted in Figures 6 and 7. Radiative equilibrium wall temperatures at the stagnation point range from approximately 1780 K to 2200 K for all cases. Equilibrium values of temperature behind the shock are approximately 10000 K; however, nonequilibrium values for the heavy particle translational temperature  $T_h$  can briefly exceed 30000 K. The depth of the nonequilibrium region of the flow for both the aerobrake and capsule missions at all entry velocities was minimal, constituting no more than approximately 10 percent of the shock layer thickness. A similar effect was seen in the profiles for the Lunar return aerobrake (Figure 8) and capsule (Figure 9). Note that the shock layer thickness is greater in all capsule missions than in corresponding aerobrake missions. Even though the capsule has a smaller diameter than the aerobrake, its nose radius is in fact larger than the aerobrake.

Radiative emission profiles are plotted in Figures 10 to 13. The pattern of the emission profiles corresponded closely to the temperature profiles, as would be expected. The values for the stagnation radiative heat transfer are tabulated in Table 2.

The comparison between the Gordiets model for homonuclear dissociation and the standard baseline LAURA models yielded remarkably similar profiles. The convective heat transfer profiles in Figure 14 are indistinguishable. The only significant difference in the two models was found in their temperature profiles (Figure 15), with the or Gordiets model having a slightly lower  $T_H$  at

peak and a correspondingly higher  $T_V$  peak value. This resulted in an enhanced radiative emission profile as seen in Figure 16. The radiative heat flux to the wall at the stagnation point for the Gordiets case was  $56.85 \text{ W/cm}^2$  as opposed to the  $53.58 \text{ W/cm}^2$  for the baseline model (Table 2).

Table 2 - Radiative Heat Transfer at Stagnation

case	$q_R \text{ W/cm}^2$
la11st	53.58
lc11sh	110.99
ma11st	199.75
ma12st	448.93
ma14st	901.47
mc11sh	184.26
mc12sh	458.40
mc14sh	1178.4

## CONCLUSIONS

The aerothermal environment is examined for two vehicle forebodies near the peak heating points of Lunar and Martian return-to-Earth trajectories at several nominal entry velocities. The first vehicle forebody is that of a  $70^\circ$  aerobrake with 13.7 m diameter for entry into Earth orbit; the second, a capsule of Apollo configuration with 3.95 m diameter for direct entry into the Earth's atmosphere. The configurations and trajectories are considered likely candidates for such missions. Two-temperature, thermochemical nonequilibrium models are used in the flowfield analyses. In addition to Park's empirical model for dissociation under conditions of thermal nonequilibrium, the Gordiets kinetic model for the homonuclear dissociation of  $N_2$  and  $O_2$  is also considered. Temperature and emission profiles indicate nonequilibrium effects in a 2 to 5 cm post shock region. Substantial portions of the shock layer flow appear to be in equilibrium. The shock layer over an aerobrake for return from the moon exhibits the largest extent of nonequilibrium effects of all considered missions. Differences between the Gordiets and Parks kinetic model were generally very small for the lunar return aerobrake case, the greatest difference of 6.1% occurring in the radiative heating levels.

## REFERENCES

- [1] Weilmuenster, K. James; Gnoffo, Peter A.; and Greene, Francis A.: "Navier-Stokes Simulations of Orbiter Aerodynamic Characteristics Including Pitch Trim and Bodyflap," Journal of Spacecraft and Rockets, Vol. 31, No. 3, May-June 1994, pp 355-366.
- [2] Gnoffo, Peter A.; Weilmuenster, K. James; Braun, Robert D.; and Cruz, Christopher T.: "Effects of Sonic Line Transition on Aerothermodynamics of the Mars Pathfinder Probe," AIAA Paper 95-1825, June 1995.

- [3] Stewart, D. A.; Rakich, J. V.; and Lanfranco, M. J.: "Catalytic Surface Effects Experiment on Space Shuttle," AIAA Paper 81-1143, June 1981.
- [4] Gupta, R. N.; Moss, J. N.; Simmonds, A. L.; Shinn, J. L.; and Zoby, E. V.: "Space Shuttle Heating Analysis with Variation in Angle of Attack and Catalycity," Journal of Spacecraft and Rockets, Vol.21, No. 2, March-April 1984, pp 217-219.
- [5] Gnoffo, Peter A.; Weilmuenster, K. James; and Alter, S. J.: "Multiblock Analysis for Shuttle Orbiter Re-entry Heating from Mach 24 to Mach 12," Journal of Spacecraft and Rockets, Vol. 31 , No. 3, May-June 1994, pp 367-377.
- [6] Gnoffo, Peter A.; Hartung, Lin C.; and Greendyke, Robert B.: "Heating Analysis for a Lunar Transfer Vehicle at Near-Equilibrium Flow Conditions," AIAA Paper 93-0270, January 1993.
- [7] Park, Chul: Nonequilibrium Hypersonic Aerothermodynamics, John Wiley & Sons, Inc., New York, 1990.
- [8] Analysis of Russian Experimental Investigations for Validation of Kinetic Models for Hypersonic Flows in Thermochemical Nonequilibrium, Edited by G. G. Chernyi and S. A. Losev, Final Report for Research Grant No. 93-0987-01, North Carolina State University, July 1993.
- [9] Schonemann, A. T.; Auweter-Kurtz, M.; Habiger, H. A.; Sleziona, P. C.; and Stockle, T.: "Analysis of the Argon Additive Influence on a Nitrogen Arcjet Flow" Journal of Thermophysics and Heat Transfer, Vol. 8, No. 3 , July-September, 1994, pp 466-472.
- [10] Sharma, S.; Ruffin, S. M.; Gillespie, W. D.; and Meyer, S. A.: "Nonequilibrium Vibrational Population Measurements in an Expanding Flow Using Spontaneous Raman Spectroscopy," AIAA Paper 92-2855, July 1992.
- [11] Sharma, S.; Ruffin, S. M.; Gillespie, W. D.; and Meyer, S. A.: "Nonequilibrium Vibrational Population Measurements in an Expanding Flow Using Spontaneous Raman Spectroscopy," AIAA Paper 92-2855, July 1992.
- [12] Cauchon, D. L.: "Radiative Heating Results from the Fire II Flight Experiment at a Reentry Velocity of 11.4 Kilometers per Second," NASA TM X-1402, 1966.
- [13] Erdman, Peter W.; Zipf, Edward C.; Espy, Patrick; Howlett, L. Carl; Levin, Deborah A.; Collins, Robert J.; and Candler, Graham V.: "Measurements of Ultraviolet Radiation from a 5-km/s Bow Shock," Journal of Thermophysics and Heat Transfer, Vol. 8, No. 3 , July-September, 1994, pp 441-446.
- [14] Gnoffo, Peter A.; Gupta, Roop N.; and Shinn, Judy: "Conservation Equations and Physical Models for Hypersonic Air Flows in Thermal and Chemical Nonequilibrium," NASA TP 2867, February 1989.
- [15] Gnoffo, Peter A., "Point-Implicit Relaxation Strategies for Viscous, Hypersonic Flows," in Computational Methods in Hypersonic Aerodynamics, T.K.S. Murthy, ed., Computational Mechanics Publications, Kluwer Academic Publishers, pp 115-151, 1991.

- [16] Cheatwood, F. M., and Gnoffo, P. A., "A User's Manual for the Langley Aerothermodynamic Upwind Relaxation Algorithm (LAURA)," NASA TM 4674, 1995.
- [17] Park, Chul; Howe, John T.; Jaffe, Richard L.; and Candler, Graham V.: "Chemical-Kinetic Problems of Future NASA Missions ", AIAA 91-0464, January 1991.
- [18] Losev, S.A.; Makarov, V. N.; Pogosbekyan, M. J.; and Shatalov, O. P.: "Thermochemical Nonequilibrium Kinetic Models in Strong Shock Waves on Air," AIAA 94-1990, June 1994.
- [19] Weilmuenster, K. James; and Gnoffo, Peter A.: "Solution Strategies and Heat Transfer Calculations for Three-Dimensional Configurations at Hypersonic Speeds," AIAA 92-2921, July, 1992.
- [20] Moreau, S.; Laux, C. O.; Chapman, D. R.; and MacCormack, R. W.: "A More Accurate Nonequilibrium Air Radiation Code: NEQAIR Second Generation," AIAA 92-2968, July 1992.

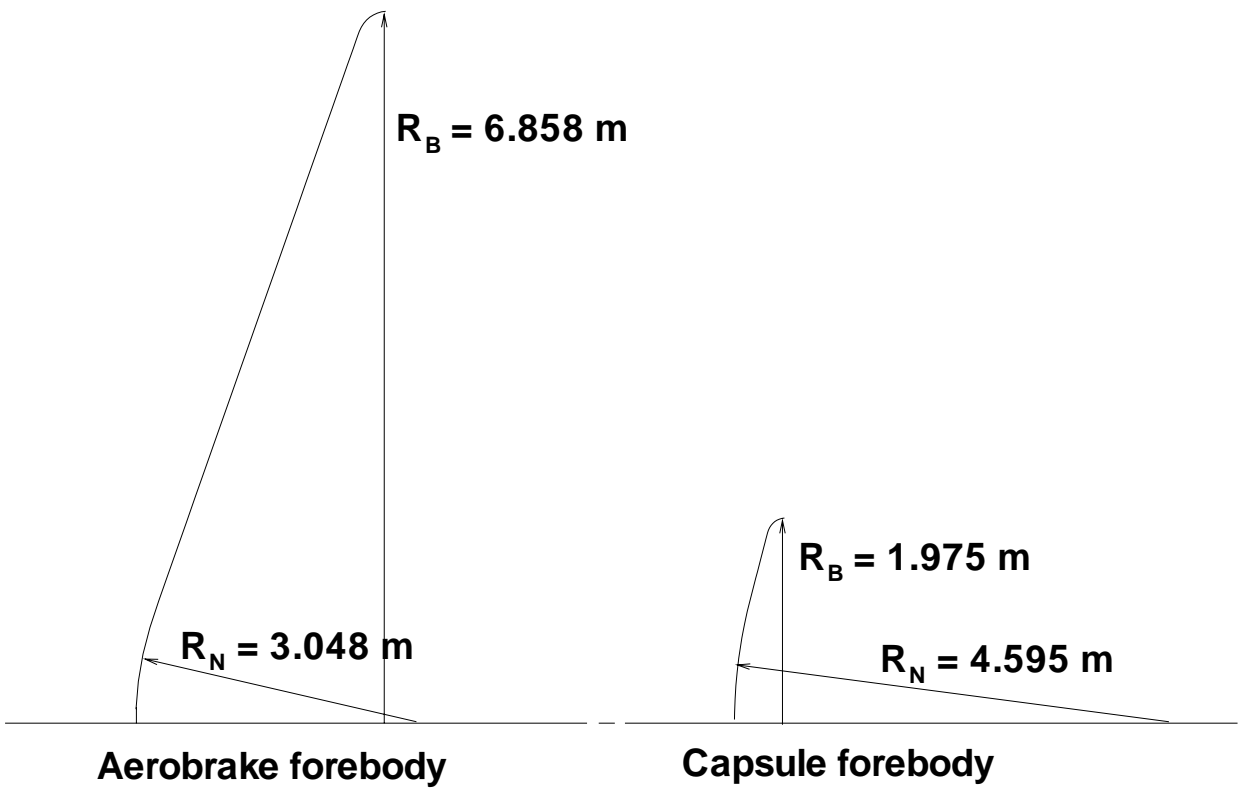


Figure 1: Aerobrake and capsule geometries.

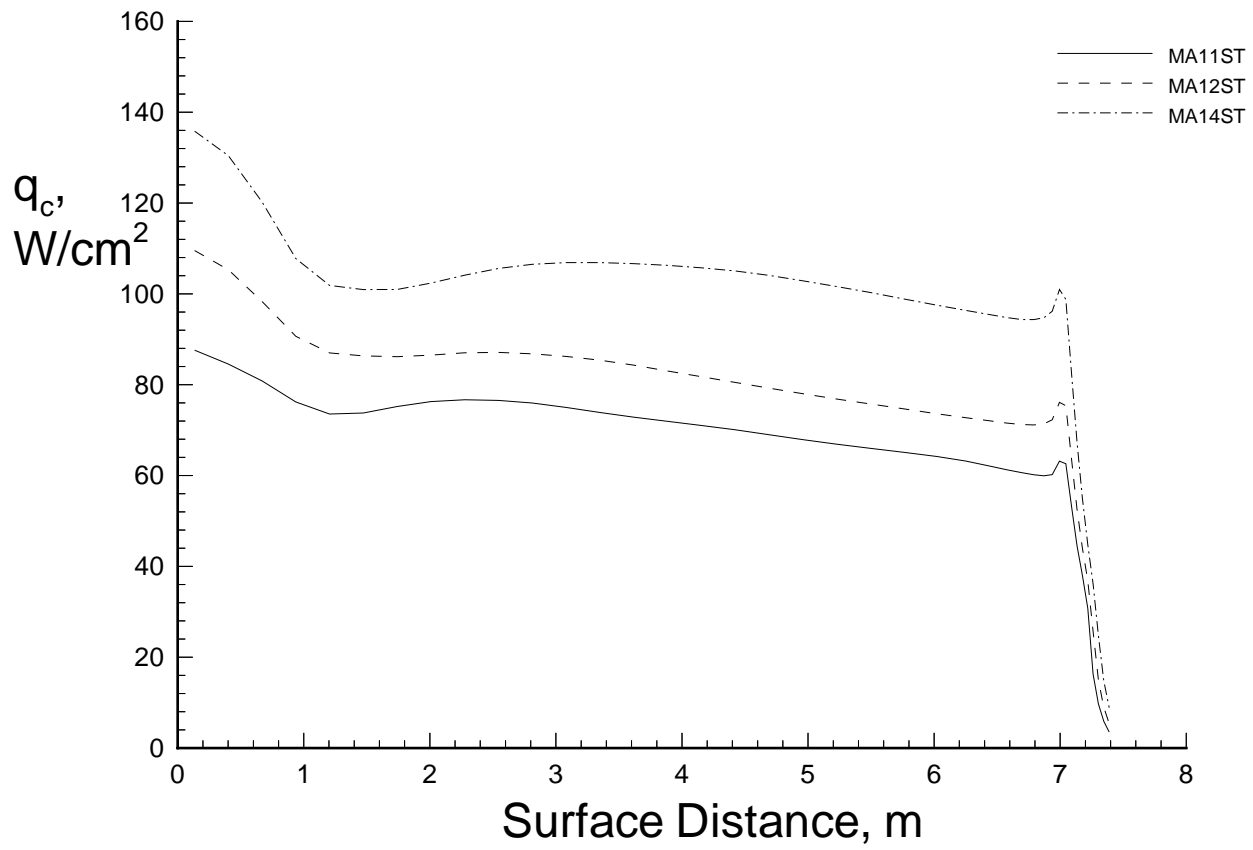


Figure 2: Convective heating profiles for the Martian return aerobrake.

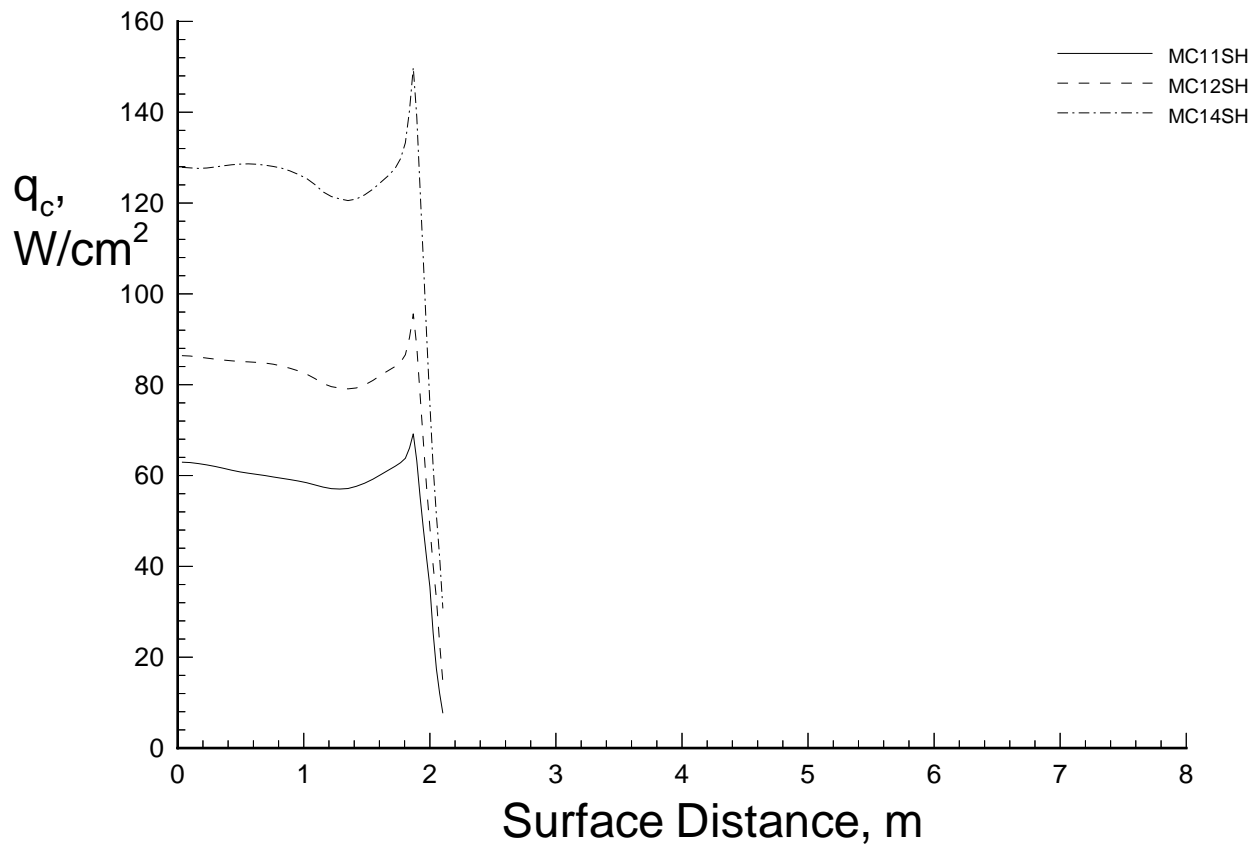


Figure 3: Convective heating profiles for the Martian return capsule.

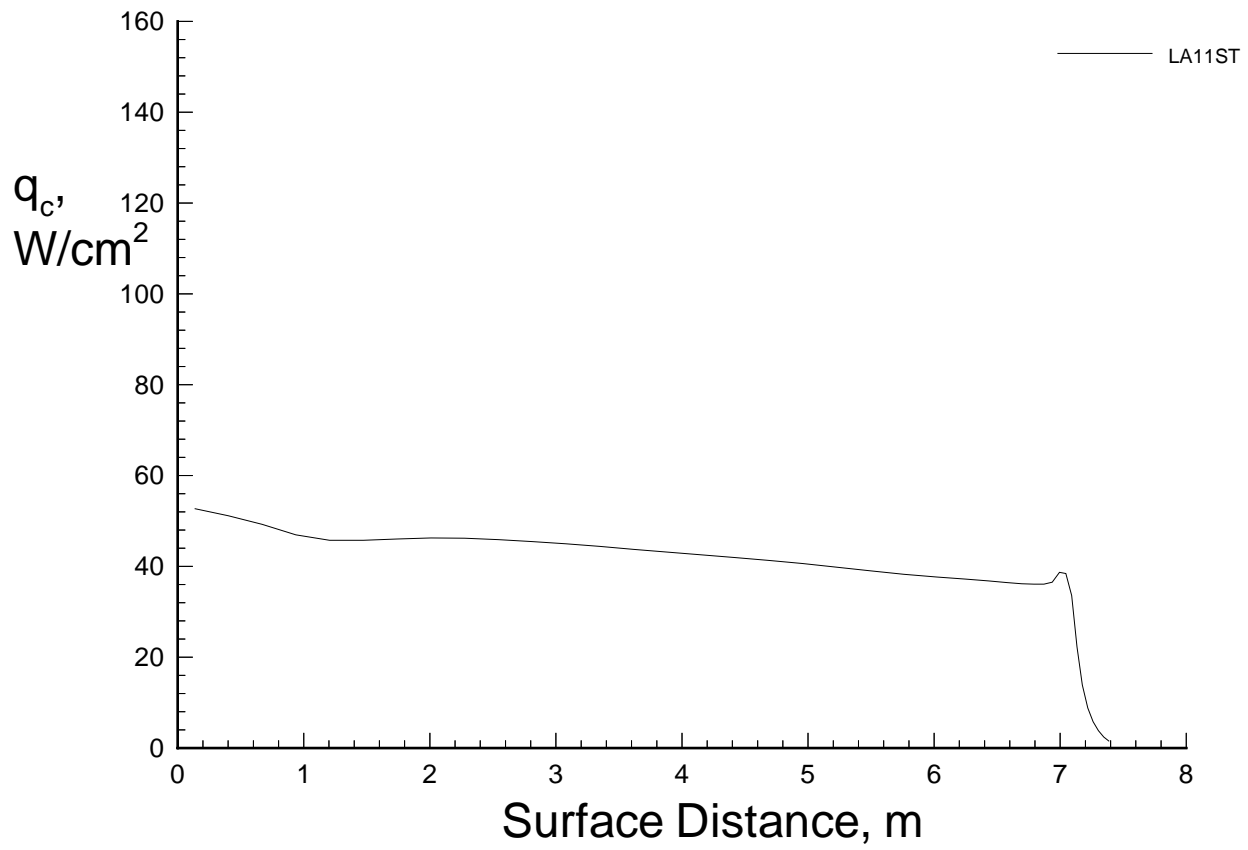


Figure 4: Convective heating profile for the Lunar return aerobrake.

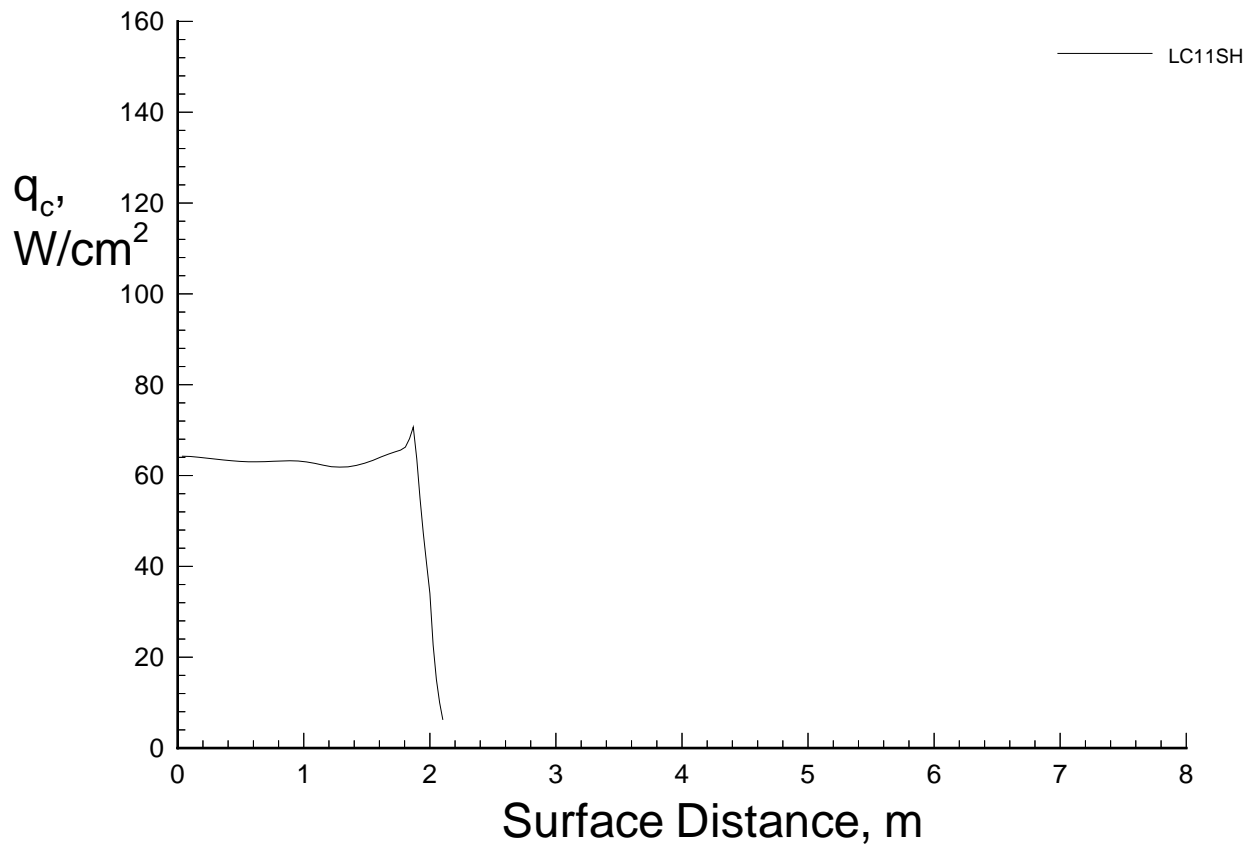


Figure 5: Convective heating profile for the Lunar return capsule.

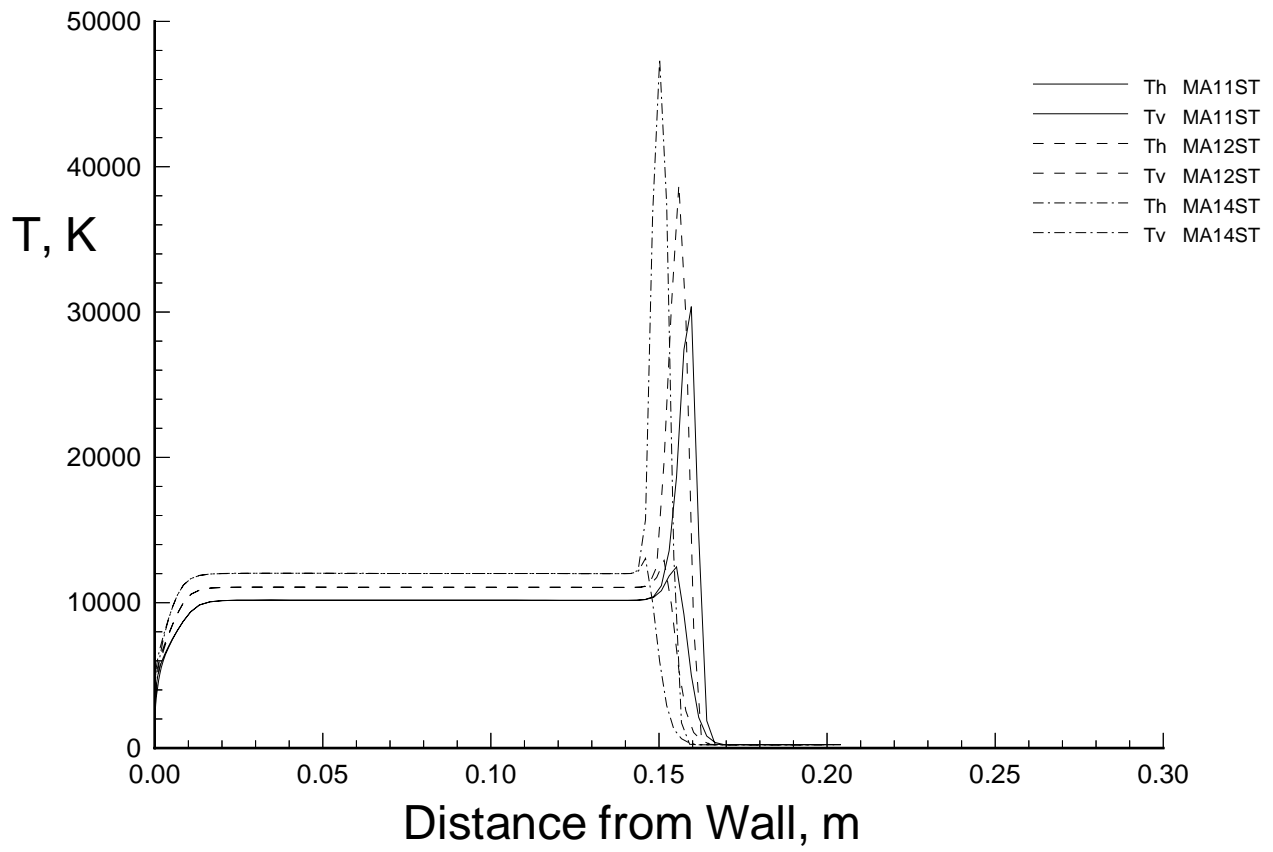


Figure 6: Temperature profiles for the stagnation streamline of the Martian return aerobrake.

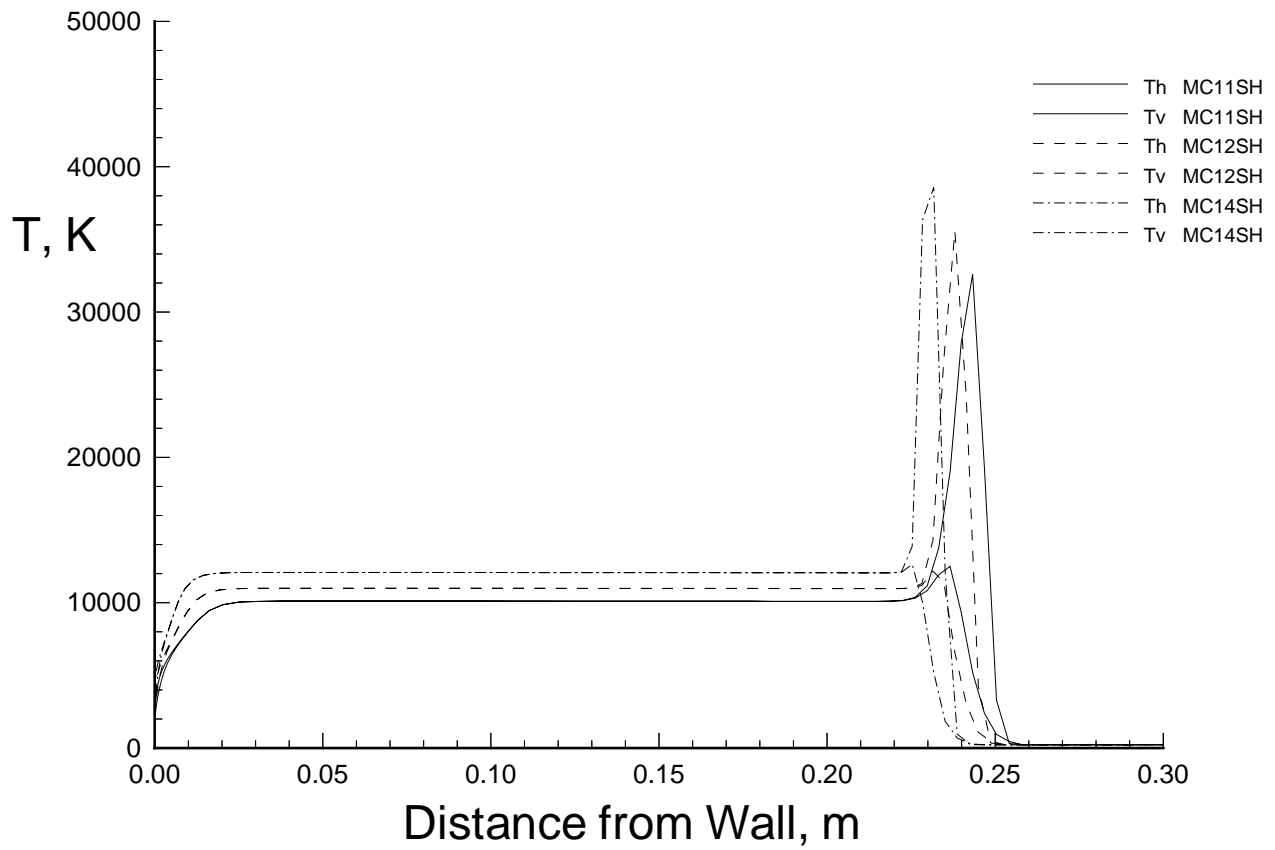


Figure 7: Temperature profiles for the stagnation streamline of the Martian return capsule.

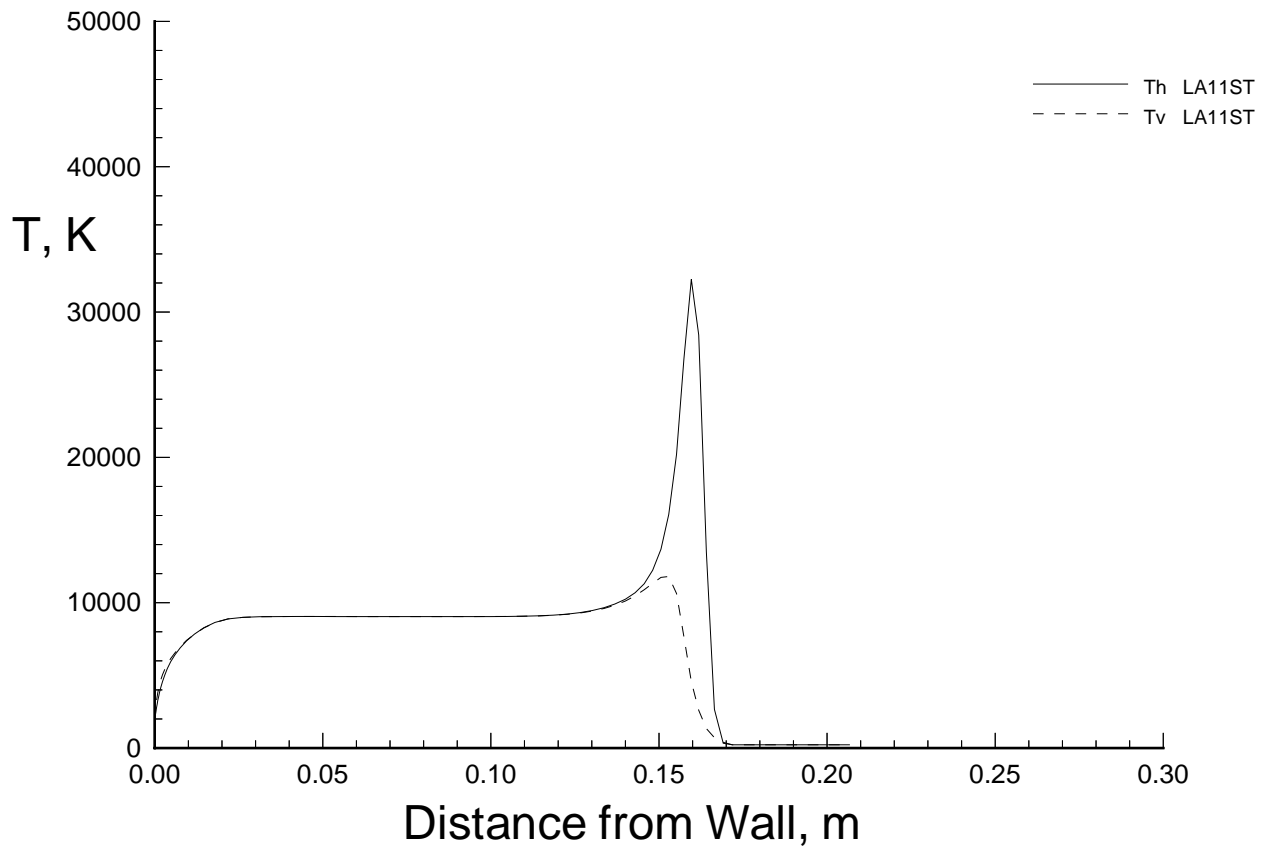


Figure 8: Temperature profile for the stagnation streamline of the Lunar return aerobrake.

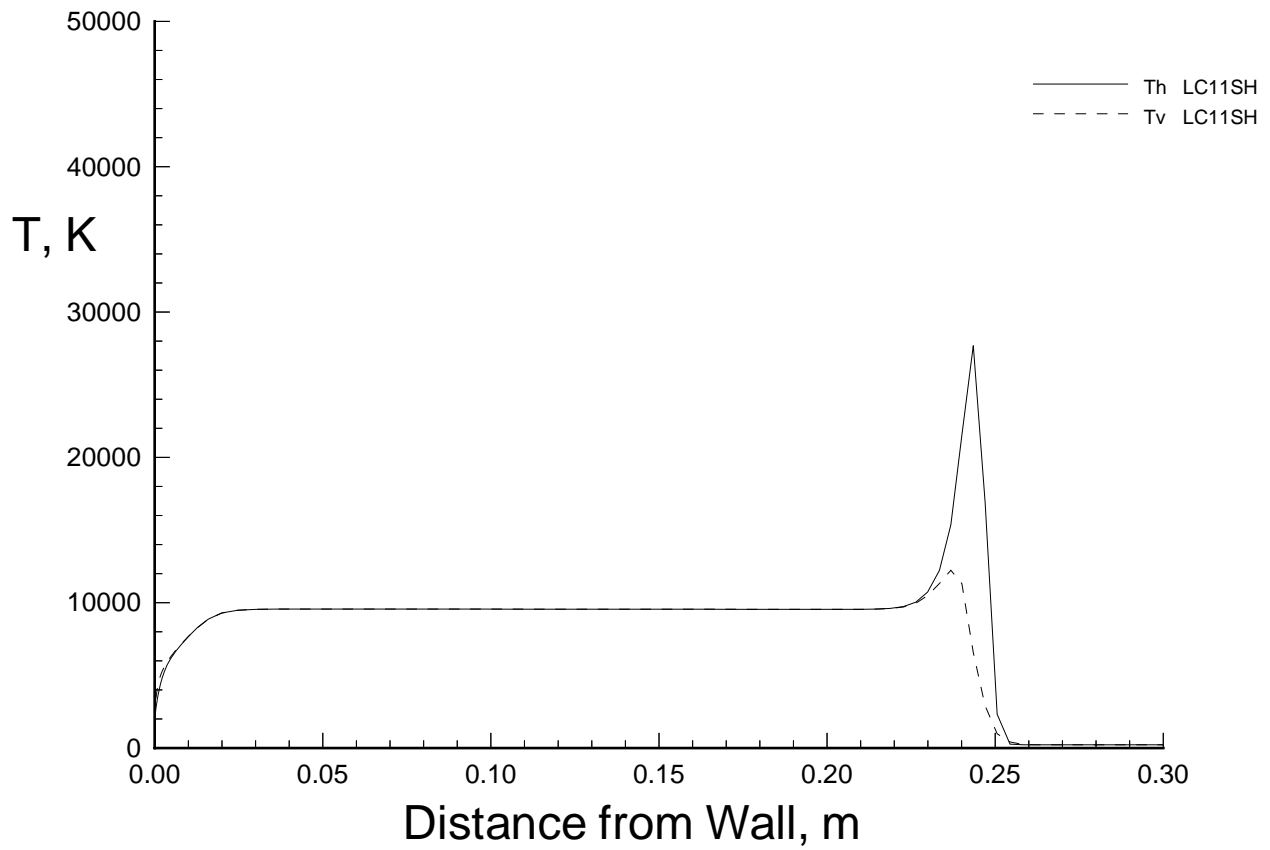


Figure 9: Temperature profile for the stagnation streamline of the Lunar return capsule.

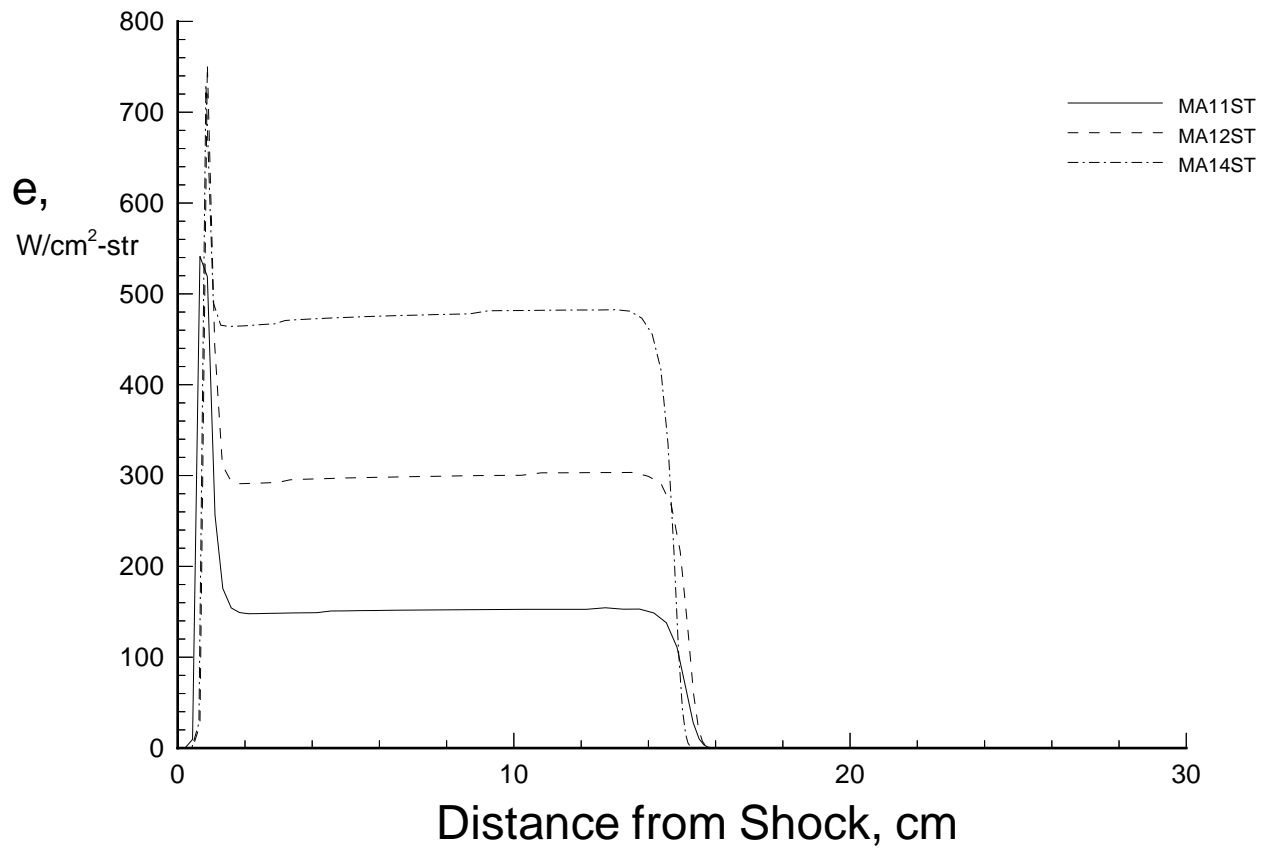


Figure 10: Radiative emission profiles for the Martian return aerobrake stagnation streamline.

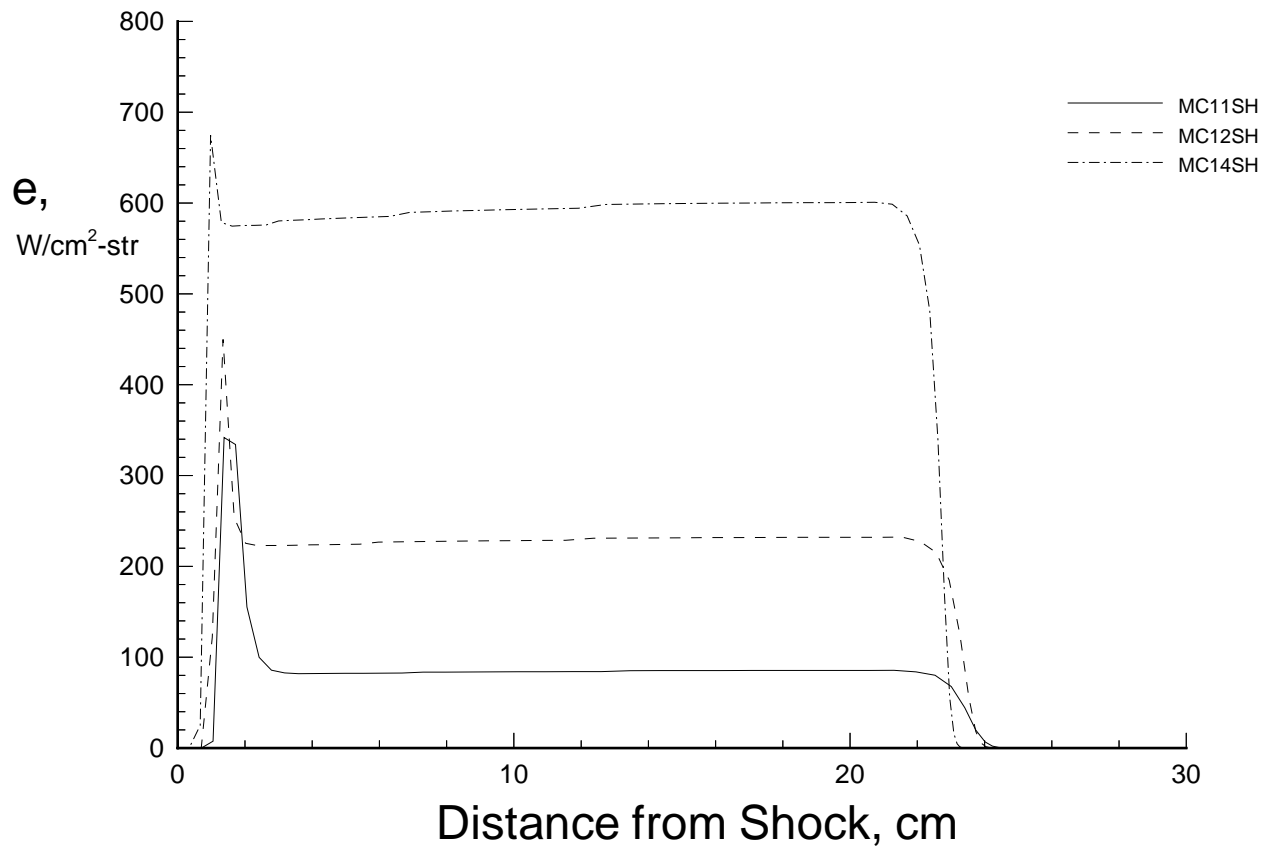


Figure 11: Radiative emission profiles for the Martian return capsule stagnation streamline.

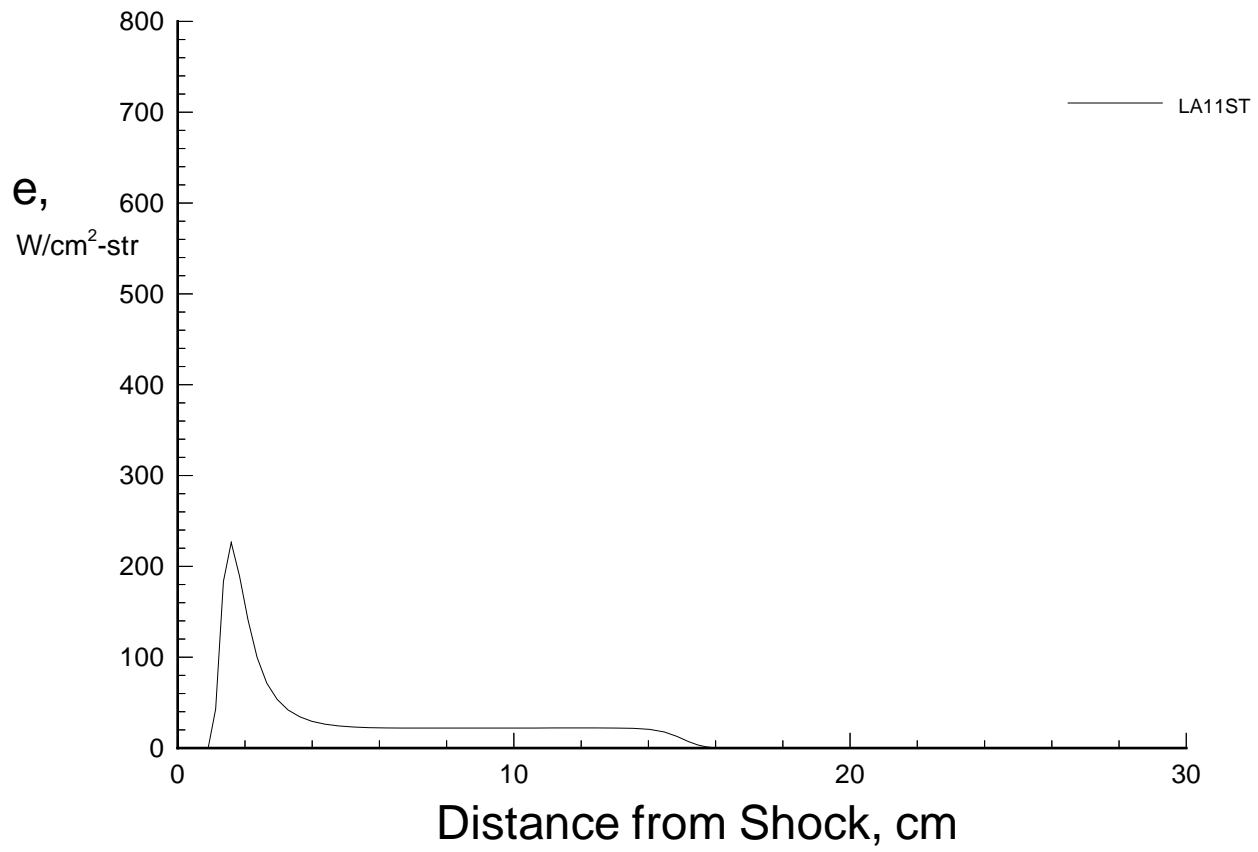


Figure 12: Radiative emission profile for the Lunar return aerobrake stagnation streamline.

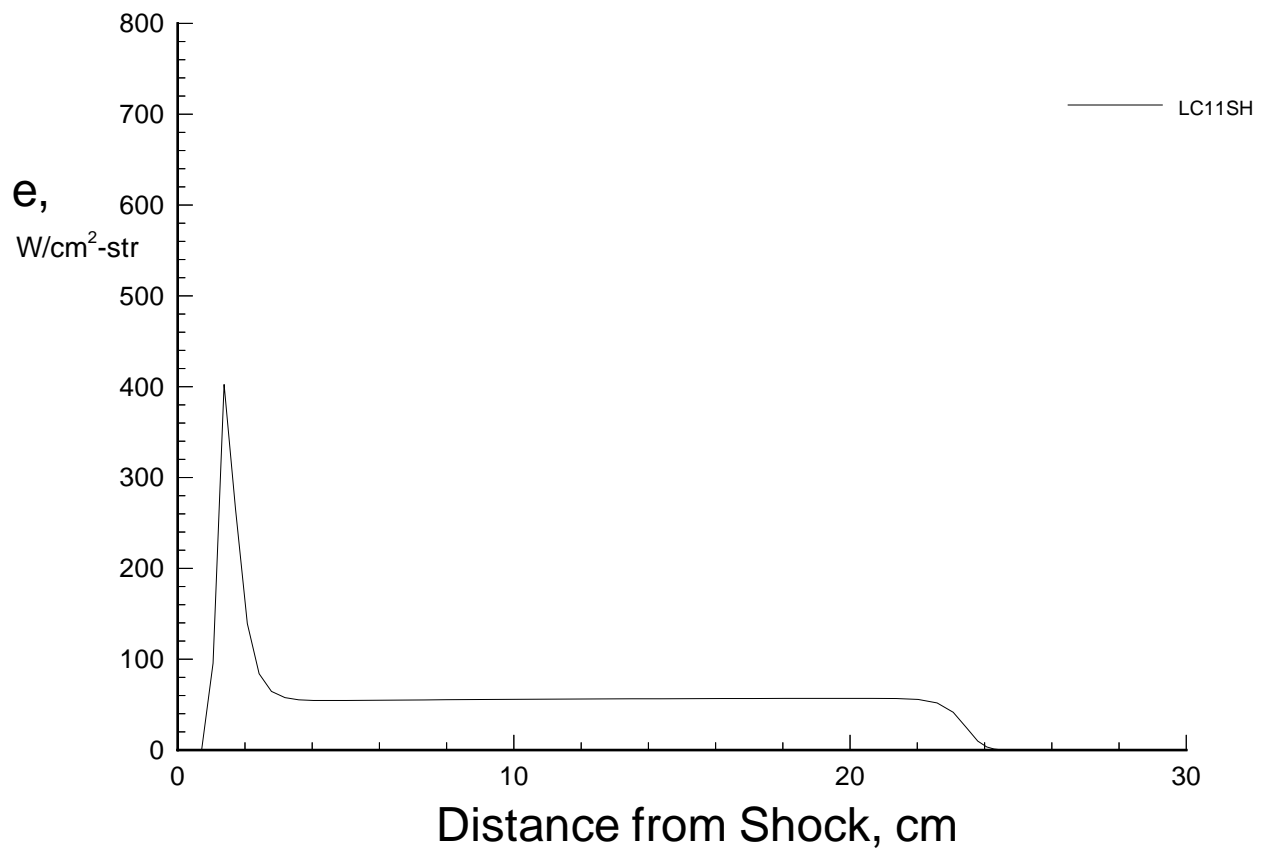


Figure 13: Radiative emission profile for the Lunar return capsule stagnation streamline.

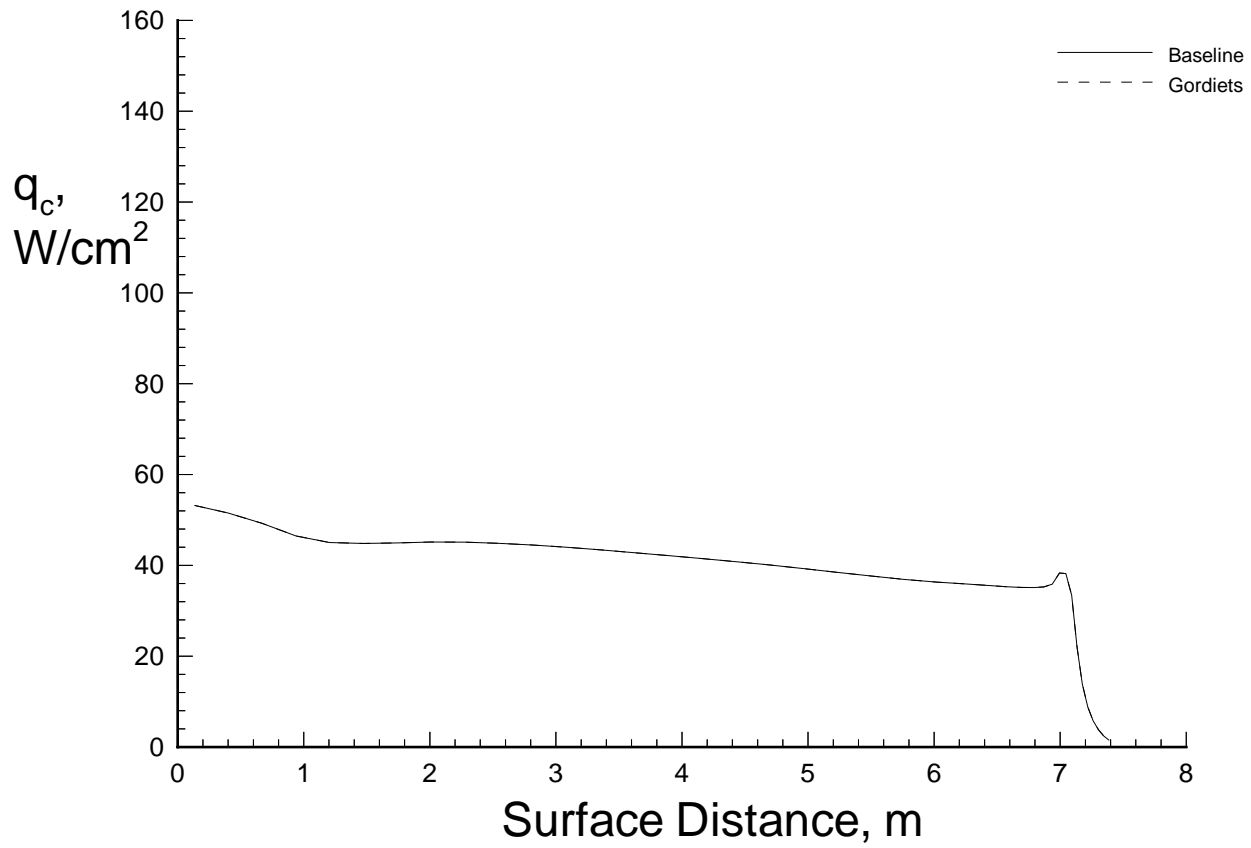


Figure 14: Convective heat profile comparison between the baseline LAURA and Gordiets model - Lunar return aerobrace.

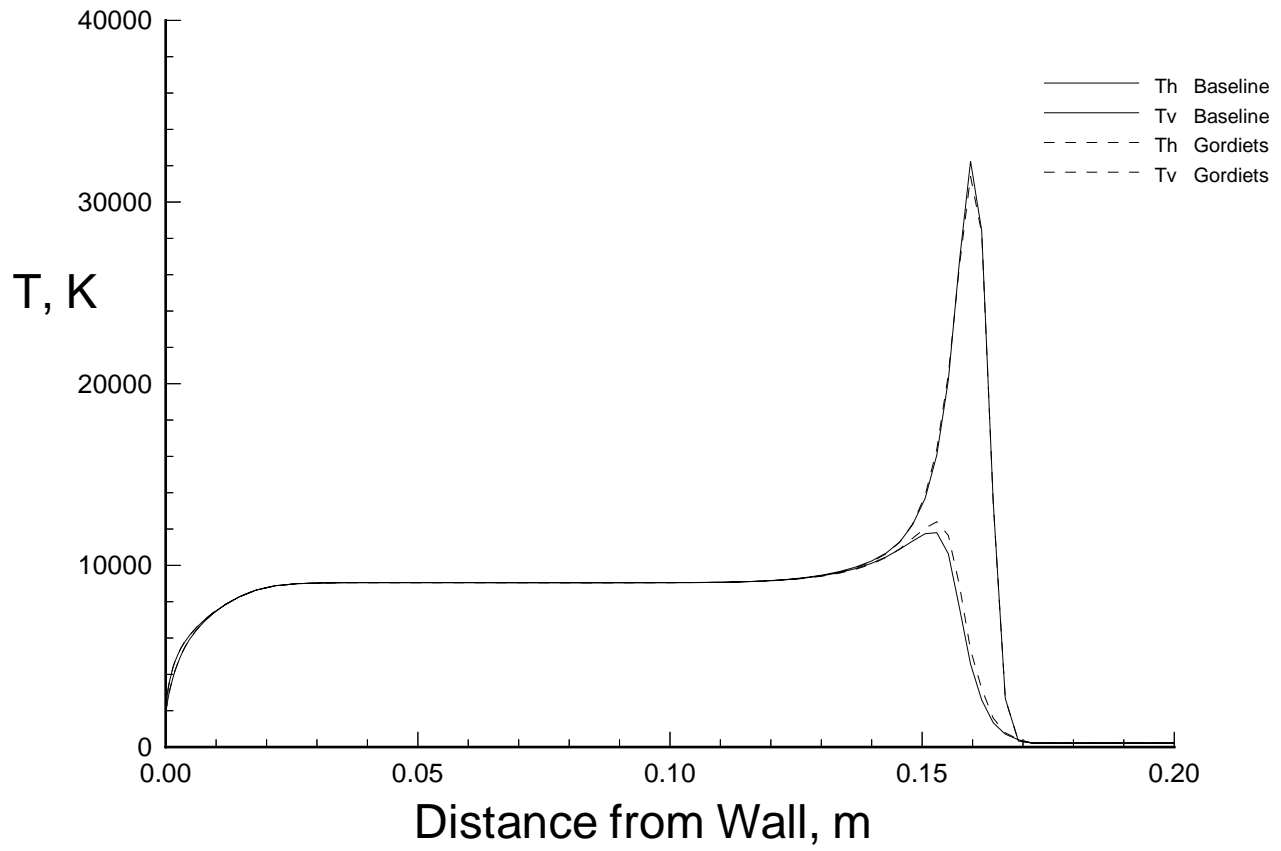


Figure 15: Stagnation streamline temperature profile comparison between the baseline LAURA and Gordiets model - Lunar return aerobrake.

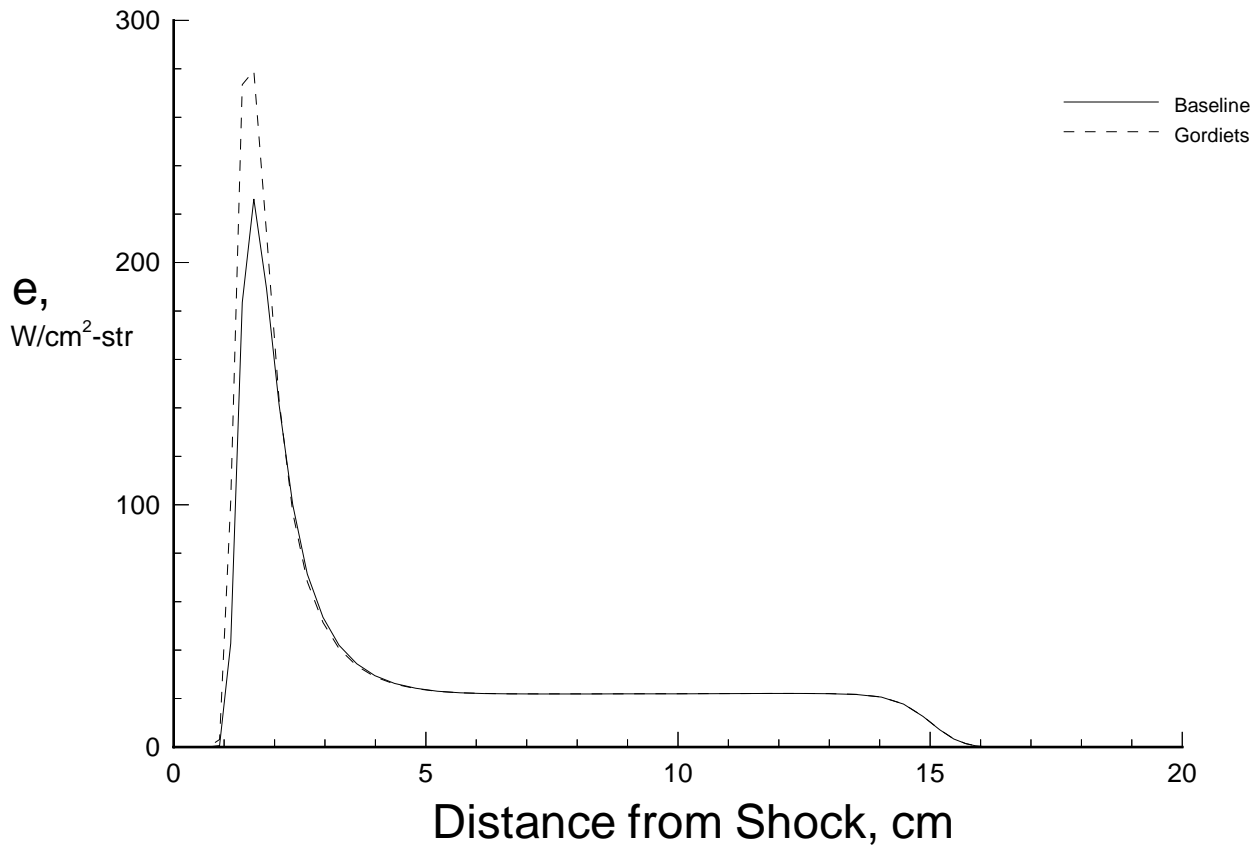


Figure 16: Stagnation streamline radiative emission profile comparison between the baseline LAURA and Gordiets model - Lunar return aerobrace.